Phosphates form spectroscopically dark state assemblies in common aqueous solutions

Joshua S. Straub[a,1], **Mesopotamia Nowotarski**[b,1], **Jiaqi Lu**[c], **Tanvi Sheth**[d], **Matthew P.A. Fisher**[a], **Matthew E. Helgeson**[d], **Alexej Jerschow**[c,2], **and Songi Han**[b,d,2]

[a]Department of Physics, University of California, Santa Barbara, CA 93106-9530; [b]Department of Chemistry, University of California, Santa Barbara, CA 93106-9510; [c]Department of Chemistry, New York University, New York, NY 10003; [d]Department of Chemical Engineering, University of California, Santa Barbara, CA 93106-5080

This manuscript was compiled on August 16, 2021

Phosphates and polyphosphates play ubiquitous roles in biology as integral structural components of cell membranes (1, 2) and bone (3–5), or as vehicles of energy storage via adenosine triphosphate (6, 7) and phosphocreatine (8, 9). The solution phase space of phosphate species appears more complex than previously known. We present NMR and cryogenic transmission electron microscopy (cryo-TEM) experiments that suggest phosphate species including orthophosphates, pyrophosphates and adenosine phosphates associate into dynamic assemblies in dilute solutions that are spectroscopically 'dark'. Cryo-TEM provides visual evidence of formation of spherical assemblies tens of nanometers in size , while NMR indicates that a majority population of phosphates remain as individual ions in exchange with these assemblies. As temperature is increased, these assemblies grow in population and can be further modulated by salt type, salt concentration and molecular crowding. Diffusion Ordered Spectroscopy (DOSY) verifies the shedding of hydration water of orthophosphates with increasing temperature. The formation of these assemblies is reversibly and entropically driven by the partial dehydration of phosphate groups, indicating a thermodynamic state of assembly held together by multivalent interactions between the phosphates. This study presents the surprising discovery that phosphate molecules ubiquitously present in the biological milieu can readily form dynamic assemblies and networks largely invisible to NMR spectroscopy under a wide range of solution conditions, highlighting a hitherto unreported property of phosphate's native state in biological systems and solutions.

Phosphate | Assembly | Dark State | Dehydration

Phosphate containing species are in constant flux throughout the phosphorus cycle and are pooled within the cells of all living organisms. Cellular energy is primarily harvested through dynamical formation and breakage of phosphoanhydride chemical bonds of adenosine phosphates (6, 7). In a different biological context, free phosphates and their subsequent assembly are involved in bone formation and growth (3–5). However, these biological processes are not well understood. An understanding of the equilibrium between free phosphates and higher-order phosphate species in the form of polyphosphates and phosphate clusters would be key to the manipulation of biological energy and/or the engineered assembly of biological structures.

^{31}P nuclear magnetic resonance (NMR) offers useful information about the composition, dynamics and structural properties of lipid membrane interfaces (10–12), phosphorylated biomolecules (13–15), polyphosphates (16, 17) and precursors of bone formation (18). We performed ^{31}P NMR to investigate the native state of phosphate species as a function of temperature with the initial intent to subsequently study the formation processes of calcium phosphate clusters. In this process, we encountered peculiar ^{31}P NMR line broadening with increasing temperature of aqueous solution of pure phosphates. Such characteristics cannot be explained by the usual temperature dependent T_2 relaxation due to increasing molecular tumbling of small molecules. ^{31}P NMR line broadening as a function of pH, phosphate concentration, and counter cation species has been described in the literature (19–21), however line broadening with increasing temperature has not been discussed previously.

Based on these unexpected results, we present experimental results showing that phosphate containing species, including orthophosphate, pyrophosphate, and adenosine diphosphate assemble into hitherto unreported spectroscopically 'dark' species, whose fractional population increases with increasing temperature. This observation is shown to be consistent with the dehydration entropy-driven formation of dynamic phosphate assemblies. ^{31}P NMR Chemical Exchange Saturation Transfer (CEST) reveals that phosphates assemble into species with broad spectroscopic signatures, whose population is in exchange with NMR-detectable phosphate species. A sub-population of these assemblies are also observed in cryogenic transmission electron microscopy (cryo-TEM) images to exhibit droplet-like spherical assemblies up to 100 nm in diameter. The discovery that common phosphate-containing molecules can readily assemble into higher order species in water under physiological conditions in the absence of biologically

Significance Statement

We show the discovery of surprisingly complex dynamic assemblies exhibited by aqueous phosphate molecules.. These assemblies form under a wide range of biologically-relevant solution conditions and with a variety of phosphate species. Phosphates are ubiquitous in the biological milieu in the form of free phosphate ions, phosphorylated proteins, RNA, DNA, ATP, the cell membrane and calcium phosphate species en route to bone formation. Understanding the behavior of phosphate species in solution is important for understanding the many complex processes in which they are involved. Our discovery shows that phosphate species readily form assemblies in aqueous solution, which should be considered when studying their role in modulating biocatalysis, cellular energy balance or the formation of biomaterials.

Please provide details of author contributions here.

The authors declare no conflict of interest.

[1]Joshua Straub and Mesopotamia Nowotarski contribued equally to this work.

[2]Email: songihan@ucsb.edu, alexej.jerschow@nyu.edu

activated processes should be relevant to a variety of biological and biochemical processes that use phosphates as building blocks, or as an ingredient in the aqueous environment.

Results and Discussion

Unexpected NMR relaxation behavior. We measured a series of ^{31}P NMR spectra of an aqueous solution of 10 mM potassium orthophosphate at pH 4.5 as a function of temperature between 293 K and 343 K. Each spectrum consisted of a single ^{31}P NMR line that showed significant broadening with increasing temperature, as shown in Fig. 1*A*. The full width at half maximum (FWHM) linewidth increases from 1.99 to 2.62 Hz, while the chemical shift only slightly changes from -0.66 to -0.22 ppm as referenced to 85% H_3PO_4 at 293 K. To test the consistency and generality of this observation, we repeated these measurements of orthophosphate with sodium and potassium counterions at concentrations of 10 mM, 100 mM and 1 M, at varying pH from 1 to 12, and at field strengths corresponding to ^{1}H NMR frequencies of 400 MHz and 500 MHz, as shown in Fig. S1, S2A, and S3A. Under every condition tested, the general trend of ^{31}P NMR line broadening with increasing temperature was observed.

To explore this observation further, we tested a series of phosphate-containing species in addition to orthophosphates, such as pyrophosphate, adenosine diphosphate (ADP) and adenosine triphosphate (ATP), and found the phenomenon of line broadening with increasing temperature for all of these different phosphate containing species tested here (Fig. 1*B*). While the extent of ^{31}P NMR line broadening with increasing temperature varies for the different species and solution conditions, this general trend persisted, suggesting that there is a common underlying molecular mechanism for solvent-exposed phosphate groups.

This line broadening is surprising, as it is inconsistent with expected trends for small molecules, including ionic species. Increasing temperature should generally lead to motional narrowing of NMR resonances of small molecules as their tumbling rate increases. An exception to this trend would be a case where chemical exchange processes lead to a transition from an intermediate to a faster motion regime while the chemical shifts of the two species diverge, before the two exchanging resonances separate. In such a case, however, one would normally observe the splitting of the broad line into additional narrow resonances at higher temperature, which was not observed for any of the phosphate-containing species studied under a wide range of experimental conditions. An additional possibility could be scalar relaxation of the second kind, which has been observed to lead to line broadening with increasing temperature (22). However, for such a case the proton exchange rate should be of the same order of magnitude as the linewidth, i.e. on the scale of a few Hz, which is not the case for our phosphate solutions (23).

To further examine the nature of the underlying process leading to the observed line broadening and its temperature-dependence, we measured the ^{31}P NMR spin-spin relaxation rate, R_2, at varying temperatures from 293 K to 343 K. This allowed us to assess whether the ^{31}P NMR line broadening with increasing temperature originates from inhomogeneous broadening due to the presence of multiple distinct spectral components or from lifetime broadening. The value for R_2 in Hz measured by the Carr-Purcell-Meibom-Gill (CPMG)

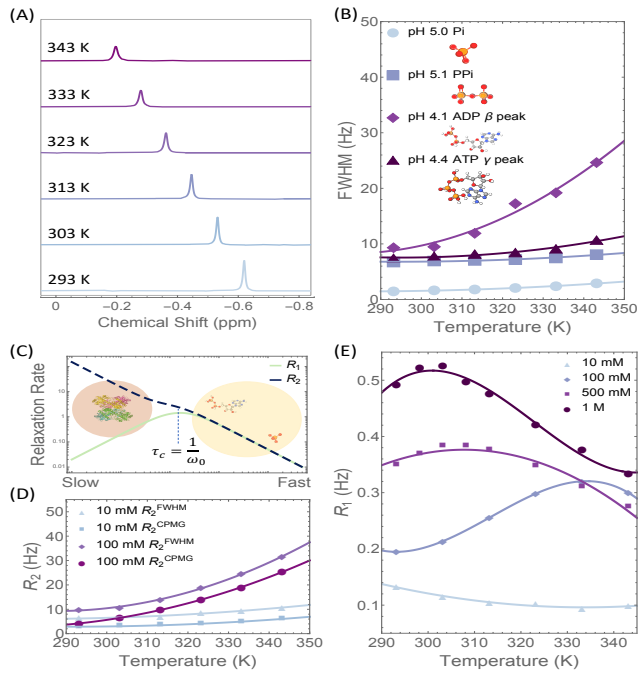

Fig. 1. P^{31}P NMR results for phosphate-containing species. (*A*) 1D NMR spectra from 10 mM sample in (*D*) and (*E*) taken at every 10 ℃ showing line broadening in orthophosphate. (*B*) Linewidths for orthophosphate, pyrophosphate, ADP, and ATP as a function of temperature showing monotonic increase with temperature. Solid lines are quadratic fits to data to guide the eye. (*C*) R_1 and R_2 curves as a function of molecular tumbling rate from Bloembergen-Purcell-Pound theory. Cartoons illustrate the approximate locations of ionic phosphate, ADP, and a standard protein based on tumbling rates. (*D*) R_2 as extracted from a CPMG pulse sequence and from FWHM for 10 mM and 100 mM monobasic potassium orthophosphate pH 4.5 as a function of temperature, showing monotonic increase in R_2 in each case. Solid lines are quadratic fits to data to guide the eye. (*E*) R_1 for 10 mM, 100 mM, 500 mM, and 1 M monobasic potassium orthophosphate pH 4.5 as a function of temperature showing different curve shapes as a function of concentration. Solid lines are quadratic (10 mM, 500 mM) or cubic (100 mM, 1 M) fits to data to guide the eye.

(24, 25) sequence was compared to that extracted from the FWHM (following $R_2 = \pi \cdot$ FWHM) for a 10 mM and 100 mM solution of potassium orthophosphate, as shown in Fig. 1*D*. We found that the two closely tracked each other, with slightly higher values for the FWHM-derived, compared to the directly measured via R_2. This observation verified that the phosphate linewidth is primarily broadened by the dynamical properties of a homogeneous spectral population. This correspondence was found consistently across all samples tested. The expected trend from Bloembergen-Purcell-Pound theory (26) of decreasing R_2 with increasing molecular tumbling rate, i.e. temperature, is shown in Fig. 1*C*.

The temperature-dependence of the spin-lattice relaxation rate, R_1, provides further information on the molecular-scale dynamical properties of the same set of samples under the same conditions. Again, wholly unexpected values and trends were found. As illustrated in Fig. 1*C*, small molecular species tumble in the 'fast' regime, and so R_1 is expected to monotonically decrease with increasing temperature, and to coincide closely with the R_2 values. We found that the R_1 values for orthophosphates at concentrations from 10 mM to 1 M are as many as two orders of magnitude smaller than the R_2 values of the same samples, even at 293 K. This observation suggests that a significant fraction of the phosphate species experience much slower dynamics than those of isolated orthophosphate monomers. Assuming a random field relaxation mechanism, the molecular tumbling time would have to be larger than 10 ns, corresponding to a hydrodynamic diameter of larger than 4.4 nm, in order to lead to the observed difference between R_1 and R_2.

This consideration leads to the question of whether the states of phosphates giving rise to the observed properties correspond to larger phosphate assemblies. When examining the shape of change in the R_1 with increasing temperature, we observed a subtle deviation from BPP theory near 330 K for the solution of orthophosphates at 10 mM concentration. The initial decline of R_1 with temperature is expected, but not the observed plateau at temperatures above 330 K. This latter observation is again consistent with a temperature-induced formation of larger phosphate assemblies. A similar trend is observed for several 10 mM samples over a wide range of pH values (see Fig. S2B).

The temperature dependence of R_1 for orthophosphates at higher concentrations (100 mM, 500 mM, and 1 M) showed, in contrast, a local maximum with increasing temperature, where the temperature of this maximum shifts to lower values with increasing phosphate concentration. This trend, while different from that of the 10 mM orthophosphate solution, is still is not consistent with the dynamical properties of small molecules in solution. According to the Bloembergen-Purcell-Pound theory, a local maximum in R_1 is expected only for species with rotational correlation times, τ_c, matching the inverse nuclear Larmor frequency. At 11.7 Tesla and a ^{31}P NMR frequency of $\frac{\omega_0}{2\pi} = 200$ MHz, we estimate $\tau_c = 800$ ps following $\tau_c = \frac{1}{\omega_0}$. A rotational correlation time in this range implies a particle diameter of 2 nm for a spherical object. Regardless of the exact shape of the species, this size is several fold larger than that of monomeric orthophosphates (27).

The observed temperature-dependent trends in R_1 and R_2 are consistent with the phosphate molecules assembling into larger species, with tumbling in the slow motion regime and correlation time τ_c exceeding ω_0, or with the phosphate molecules being in exchange with spectroscopically invisible species that have much higher R_1 and R_2 rates, which would again be consistent with phosphate assemblies, since there are no other constituents in the solution. Higher temperatures may facilitate the growth in population and size of such assemblies and/or accelerate the exchange, and hence enhance R_1 and R_2 of the detected ^{31}P NMR signal. It is also possible that a mixture of the two regimes is observed, in which smaller phosphate assemblies coexist with spectroscopically invisible phosphate clusters across the temperature range tested, and that heating increases the relative abundance of this invisible species. Either scenario suggests the formation of larger phosphate assemblies, with enhanced populations and/or exchange rates at elevated temperatures, yielding much greater R_2 values compared to R_1, consistent with our observation.

If such larger assemblies are forming, it is important to consider their nature, and in particular the interactions leading to their formation. One possibility could be that the new assemblies are polyphosphates formed by the enhanced formation of P-O-P bonds at elevated temperatures. The ^{31}P chemical shift for phosphates is known to shift by approximately -10 ppm with each P-O-P bond formed and by a maximum of 5 ppm based upon protonation (28, 29). This is inconsistent with our observed chemical shifts, which move systematically downfield, but only very slightly, by a maximum of 0.5 ppm when the temperature is increased from 293 K to 343 K. Hence, the observed chemical shift change is too small to be attributed to covalent bond formation. The observed 0.5 ppm chemical shift change could instead be the result of changes in the equilibrium P-O bond length, potentially induced by non-covalent association of phosphate molecules. Such changes could be mediated by hydrogen bond interactions that, in turn, can be modulated by changes in phosphate hydration. Notably, all four oxygens of the phosphate group can serve as hydrogen bond donors or acceptors, depending on the protonation, hydration and partial charge state of the group, hence allowing for cooperative interactions that can give rise to the formation of larger assemblies, while still maintaining rapid exchange with ionic phosphates and small clusters given their weak interactions. In any case, the species forming must either have the same chemical shift as orthophosphate ions and/or be so broad as to be rendered spectroscopically invisible.

CEST. To test whether the phosphate species are in exchange with a spectroscopically dark population, we performed chemical exchange saturation transfer (CEST) experiments. CEST provides a means of identifying signatures of exchangeable species far below NMR detection limits. This effect is achieved by saturating a selected region in the spectroscopically invisible region of the spectrum, followed by the detection of the (visible) signal of a major species (in this case, monomeric phosphates) that is in exchange with the species below the NMR detection limit. Repeating these experiments with different saturation frequencies across the complete spectral region and power of interest permits scanning of a complete spectrum for potentially exchanging species. This procedure has been widely employed, for example, to identify weakly populated states of peptides and proteins whose protons are in exchange with water(30, 31), and in this context referred to as DEST (for dark state exchange saturation transfer)(32). The sensitivity enhancement effect for the dark species is achieved because

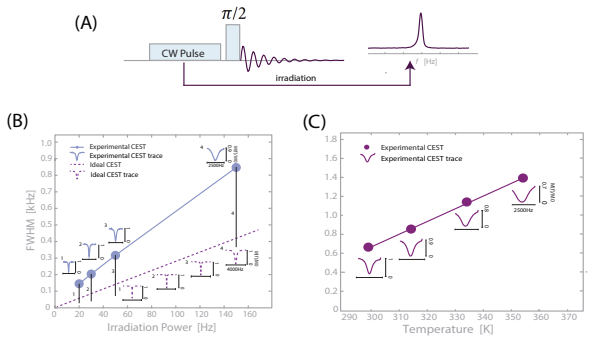

Fig. 2. ^{31}P CEST results for 100 mM orthophosphate in D_2O (pH=9.5). (*A*) CEST pulse sequence, (*B*) CEST dip width at half height as a function of CEST irradiation power of 20 Hz, 30 Hz, 50 Hz and 150 Hz at T=298.15 K, (*C*) CEST dip width at half height as a function of temperature of 298 K, 313 K, 333 K, 353 K with irradiation power of 150 Hz

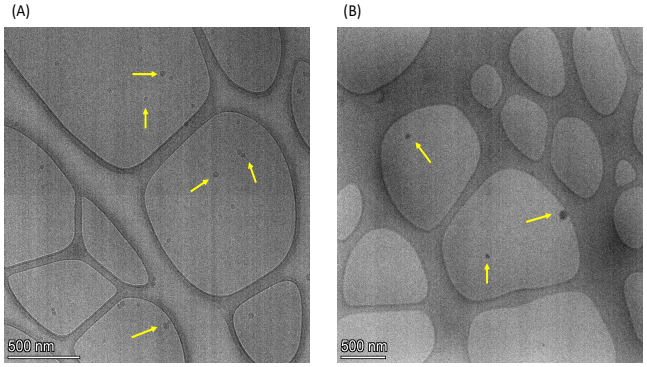

Fig. 3. TEM images of phosphate assemblies (yellow arrows) after heating phosphate solutions show droplet-like features forming at 50-100 nm in size. (*A*) 100 mM ADP heated to 343 K before vitrification. (*B*) 500 mM potassium phosphate heated to 343 K.

exchange can occur many times during the saturation pulse, and thereby transfer saturation levels between the visible and invisible species repeatedly. In the CEST experiment of this study, we recorded ^{31}P NMR spectra of the visible ^{31}P NMR signals following weak and long rf irradiation at a specified resonance frequency in what can be seen as a one-dimensional pump-probe experiment. Here, the pump frequency is stepped through a frequency range of approximately 2000 Hz, centered around the one visible ^{31}P NMR peak. In this fashion, CEST can test for the existence of spectroscopic dark states that are in exchange with phosphate species at frequencies within the scanned range.

Fig. 2 shows the measured CEST dip as a function of rf saturation power of the CEST pump irradiation, and at a series of different temperatures, of a solution of 100 mM orthophosphate. In the absence of exchange, one expects the width of the dip in the CEST spectrum to be approximately a factor two larger than the rf saturation bandwidth (expressed in Hz) (33). BY contrast, we observed that the dip widths range from 800 Hz to almost 1500 Hz, i.e., up to an order of magnitude larger than expected based on the irradiation bandwidth of 150 Hz. Furthermore, the dip widths in the CEST spectrum increased monotonically with temperature. These results suggest that exchange occurs with a population exhibiting a broad spectroscopic signature, invisible by direct spectroscopic detection at all measured temperatures. This population giving rise to the broad spectroscopic signature appears to be increasing in abundance with temperature. This outcome further validates the hypothesis that orthophosphates form assemblies, some of which are spectroscopically invisible, and are in dynamic exchange with the detectable phosphate species. Similar results were also found for CEST results from ADP samples (Fig. S4), suggesting that this behavior may be general to other phosphate species in solution.

Cryo-TEM. While the evidence for assembly formation is clear, the previous measurements provide no information regarding structure or size of the assemblies due to their spectroscopically dark nature. We hence used cryo-TEM to determine whether the phosphates assemble into large and persistent enough clusters to be visualized. Cryo-TEM was performed on ADP and orthophosphate solutions that were vitrified after heating. Interestingly, all solutions tested showed evidence of phosphate assemblies forming at sizes ranging from 30-100 nm in diameter (Figure 3, SI Figures 5-7). These features, identified by yellow arrows, have darker contrast than the vitreous ice film, indicating a region of greater electron density, and appear to be approximately spherical in shape. Amongst the conditions tested, the abundance of assemblies appeared higher in solutions heated at 343 K for 48 hours compared to solutions that are unheated, and the highest in the sample containing 100 mM ADP compared to orthophosphate solutions. These findings are consistent with the ^{31}P NMR results, which show the greatest line broadening in ADP upon heating (Figure 1B). However, even in a 10 mM sodium phosphate solution, assemblies could be seen by cryo-TEM, albeit at much lower abundance (Fig. S7) . This, again, agrees with the noted discrepancy between ^{31}P NMR T_1 and T_2 observed in all phosphate samples, suggesting that phosphate assemblies are omnipresent. Notably, the complete phosphate population is part of or is in exchange with the phosphate assemblies, given the homogeneously broadened nature of the ^{31}P NMR line, while the phosphate assemblies seen in cryo-TEM likely only reflect a sub-population of the largest phosphate assemblies. Interestingly, the spherical shape of the assemblies suggests that they exist as liquid droplets, implying that their assembly could be driven by liquid-liquid phase separation.

DOSY NMR. Having more clearly established that larger phosphate assemblies exist in solution, we now focus on the potential mechanisms of their assembly and, in particular, the specific temperature-dependent behavior we observe. Our initial attempts toward addressing this question involved pulsed field gradient (PFG) NMR to measure the self diffusion coefficients of the ^{31}P NMR signal-bearing species, and hence their hydrodynamic diameter. Using PFG NMR, we performed Diffusion Ordered SpectroscopY (DOSY) to determine spectrally resolved self-diffusion coefficients of the ^{31}P NMR signal-bearing species. DOSY measurements were performed on a 100 mM sodium orthophosphate solution of pH 4.5 at 293 K, 343 K, and again at 293 K after cooling in order to assess reversibility of any structures formed at elevated temperatures. We observed that the phosphate species all diffuse with a single translational diffusion coefficient, as demonstrated by the linear relationship between $\mathrm{Log}(\psi)$ and the square of the gradient

strength, where ψ is the signal attenuated by molecular motion along the gradient axis (Fig. 4*A*) (34). This observation of a uniform diffusion coefficient did not change with increasing temperature. However, the diffusion coefficient significantly increased from $7.5 * 10^{-10}$ m^2/s at 293 K to $3.2 * 10^{-9}$ m^2/s at 343 K. To convert these diffusion coefficients to hydrodynamic diameters, we used the Stokes-Einstein relationship, while accounting for the increased thermal energy and the decreased viscosity of water at elevated temperature. The extracted (temperature-corrected) hydrodynamic diameters for orthophosphate ions show a reversible and significant decrease of 1.8 Å at 343 K compared to 293 K (Fig. 4*B*). Similar increases in diffusion coefficient and decreases in hydrodynamic diameter were also observed for monophosphate ions in 100 mM and 1 M potassium phosphate samples and 1 M sodium phosphate samples (Fig. S8 and S9).

Reconciling the observation of assembly of orthophosphates according to ^{31}P NMR relaxation and CEST studies with this apparent decrease in the hydrodynamic radius of orthophosphate molecules suggests that the phosphate ions experience partial dehydration at elevated temperatures, and that these partially dehydrated phosphate groups can more readily assemble into, and exchange with, dynamic phosphate clusters. It is known that a single deprotonated orthophosphate moiety at infinite dilution and at pH 4.4 carries 11 water molecules within its hydration shell (35). Thus we consider our ^{31}P DOSY results, which showed a decrease in hydrodynamic diameter from 6 Å to 4.2 Å, corresponding to a decrease in hydrodynamic volume of 70 Å^3. Assuming a water radius of 1.4 Å(36), this result suggests a loss of 6 hydration waters upon heating, yielding a total of 5 hydration water molecules per orthophosphate at 343 K. To further validate this analysis, we performed Molecular Dynamics (MD) simulations using the Amber GAFF forcefield with a SPCE water model to characterize the interactions between the hydration water and the sodium ions with the phosphate ion (see SI for box size and other simulation details). These calculations show a decrease of water coordination from 13.3 to 12.5 with increasing temperature from 300 K to 360 K, when integrating over the distance range from 2 Å to 4.5 Å (Figure S10). These results are consistent with the trends observed by experimental analysis of the hydration number of orthophosphates. The quantitative disagreement could be explained due to the fact that MD simulations only considered a single phosphate.

Is DOSY then detecting the phosphates within clusters directly? As discussed, phosphorus spins in these clusters undergo rapid relaxation due to their slower tumbling rates and thus have very broad resonance lines, largely invisible to ^{31}P NMR. Thus, our DOSY measurements should only be sensitive to the free phosphate ions that exist in equilibrium with these larger, spectroscopically dark, assemblies. The DOSY results reveal that free phosphate ions exchanging with the phosphate assemblies are more dehydrated at elevated temperatures, and hence likely have a greater tendency to assemble.

Examining entropy-driven assembly. What then is the driving force for the formation of soluble, non-covalent, phosphate assemblies at equilibrium that are reversibly promoted at elevated temperature? Considering the Gibbs free energy for phosphate assembly, $\Delta G_{PA} = \Delta H_{PA} - T\Delta S_{PA}$, since generally ΔH increases with temperature (37), spontaneous phosphate assembly ($\Delta G_{PA} < 0$ requires that ΔS_{PA} must be positive, so that the entropic contribution to the free energy is heavily weighted as temperature is increased.

Possible sources for this putative entropy gain are depletion interactions, including excluded volume effects, counterion release, and/or dehydration mechanisms (38). Excluded volume interactions would not be expected to reduce the hydrodynamic diameters of individual phosphate monomers, and species with overlapping volume would co-diffuse, resulting in slower diffusion, neither of which are consistent with our DOSY results. As such, excluded volume effects cannot explain the formation of phosphate assemblies if they are driven by entropic effects.

Another commonly expected source of entropy gain upon assembly of charged species is the release of bound counterions in place of more delocalized charge interactions in the assembled state. However, potassium and sodium ions are not strongly bound to phosphate, making its release a less likely source for significant entropy increase. This assessment is consistent with our MD simulation results, which show that the counter cation number around the phosphate ion increases from 0.66 to 1.2 with increasing temperature from 300 to 360 K (see Figure S11). This analysis confirms that the phosphate-cation interaction is weak, and if anything increases with increasing temperature, making counterion release an unlikely driver of phosphate assembly. Furthermore, the observed changes in the hydrodynamic diameter of orthophosphates with increasing temperature as measured by DOSY are very similar between potassium and sodium phosphate samples (Fig. 4*A* and Fig. S9). Since sodium and potassium ions are approximately 1 Å different in size (39), we would expect to measure a difference in the change of the hydrodynamic diameter if counterion release was a major contributor to these observed size changes.

Hence, the most likely source of increase in the total entropy is the shedding of water that is more strongly associated with the phosphate ions than with bulk water, also referred to as the hydration shell. Water forms networked hydrogen bonds to strongly solvated phosphate anions, offering ample opportunities for entropy increase upon its partial release. Indeed, DOSY experiments and MD simulations confirmed that a significant number of hydration water of anywhere between 12 – 14 can be readily released by increasing the temperature from 300 to 360 K. In fact, dehydration-driven entropy increase has been shown to be a primary driver of polyelectrolyte assembly processes in water, as reported on in a recent study(40).

Manipulation of depletion interactions. Since the experimental restuls so far suggest dehydration entropy as a driver of phosphate assembly, we designed further experiments to deliberately modulate the phosphate-water interactions by known mechanisms. Since we established a viable interpretation for the change in ^{31}P NMR linewidth and relaxation data with temperature, we rely on these robust readouts to evaluate phosphate assembly formation as a function of temperature.

One can amplify dehydration by the addition of hydrophilic molecular crowders or salting-out salts of the Hofmeister series. The introduction of molecular crowders is a common technique used to reduce the volume of solvent available for the other molecules of interest in solution, thus increasing the effective concentration of the dissolved molecule (40). A common crowding agent used in the literature is the hydrophilic polymer polyethylene glycol (PEG); its strong affinity for wa-

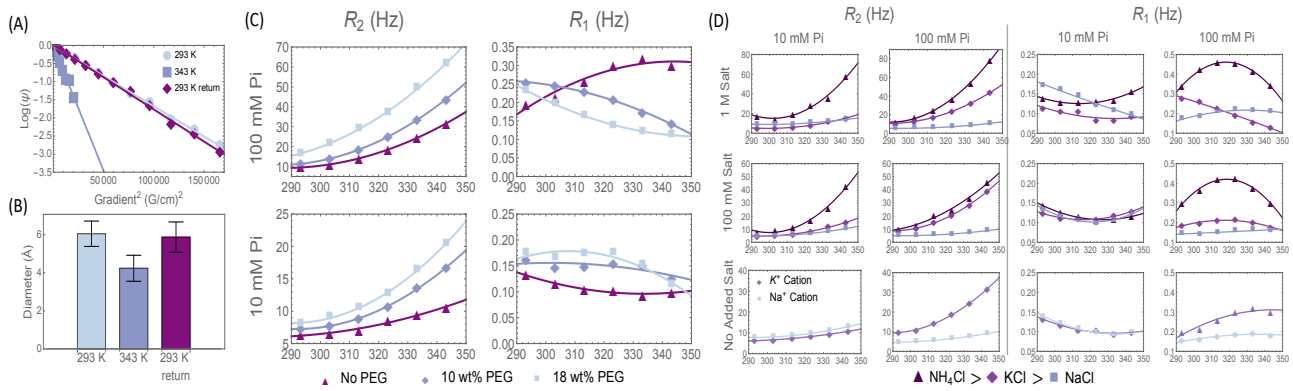

Fig. 4. Evidence of entropically driven assembly. (*A*) 100 mM sodium phosphate at pH 4.2 ^{31}P DOSY fits of Log(ψ) vs gradient strength squared show a linear relationship, indicating that a single diffusion coefficient can describe the motion. (*B*) Hydrodynamic diameters extracted from the diffusion coefficient from fits in (*A*). (*C*) R_2 and R_1 for potassium phosphate pH 4.5 in the presence of 6k MW polyethylene glycol (PEG) at varying PEG concentrations. Solid lines are quadratic fits to data to guide the eye. (*D*) R_2 and R_1 for sodium phosphate pH 4.5 samples at 10 and 100 mM, with varying cationic salt types and concentrations. Solid lines are quadratic fits to data to guide the eye. The R_2 trends follow the predicted trends for the Hofmeister series, while R_1 shows little difference at 10 mM phosphate concentration, but significant differences for different salts at 100 mM.

ter over the temperature range of interest drives dehydration and increases the effective concentration of other molecules in solution (41). ^{31}P NMR linewidth measurements measured at temperatures ranging from 293 K to 343 K indicated increased linewidth for phosphate solutions at both 10 mM and 100 mM concentrations with increasing PEG concentrations at 10 wt% and 18 wt%. This increase in linewidth cannot be accounted for solely by changes in solution viscosity from the addition of PEG (Fig. S12). This observation is thus consistent with the interpretation that PEG enhances dehydration of phosphates and subsequent clustering.

The dehydration interactions can also be modulated by the addition of various salts according to the Hofmeister series (42). This series is used in biological systems to induce salting-out (precipitation) or salting-in (dissolution) of proteins, with NH_4^+ on one salting-out end and Na^+ on the other salting-in end (43) of the series. While our phosphate clusters are not precipitated out of the solution, the magnitude of dehydration, and thus the exchange with and/or formation of assemblies, is expected to be increased with salting-out salts and decreased with salting-in salts. We applied this ensatz to our hypothesis of dehydration-driven phosphate clustering by adding in a variety of cations that enhance the tendency for salting-out tendency in the order $NH_4^+ > K^+ > Na^+$. ^{31}P NMR linewidths were measured between 293 K and 343 K for orthophosphate solutions at 10 mM and 100 mM in the presence of added chlorine salt of three different cations at 100 mM and 1 M concentrations, as well as in the absence of added salts. The extracted linewidths show that the addition of NH_4^+ causes the greatest line broadening, followed by K^+ and then Na^+, at all phosphate concentrations, salt concentrations, and temperatures (Fig. 4*D*). These results are in agreement with the predicted trend of the Hofmeister series when considering line broadening as a proxy for dehydration-induced clustering. While the R_1 results are more difficult to interpret, due to the lack of a monotonic trend, we see that the salts do change the shape and magnitude of R_1 when phosphate and/or salt concentration is high enough (Fig. 4*D*). This result is again in agreement with the hypothesis that the addition of salting-out salts impact the tendency of phosphates to cluster.

The observed effect of both PEG and cationic salts on the ^{31}P NMR linewidths adds further support to our hypothesis that dehydration entropy plays a significant role in driving the formation of the observed phosphate assemblies. Molecular crowders and salting-out cations would both serve to increase the total entropy of dehydration, further facilitated by elevated temperatures, consistent with all other ^{31}P NMR results. While chemical exchange between phosphate species of different protonation states or scalar relaxation may potentially explain some of the observed anomalous ^{31}P NMR line broadening behavior with increasing temperature, these alternative hypotheses are unable to provide comprehensive explanations for the full range of results provided here. Scalar relaxation can only dominate relaxation in a proton exchange regime many orders of magnitude away from the solutions presented here. Chemical exchange of protons on phosphate groups cannot explain the discrepancy between R_1 and R_2. And neither explanation can explain the CEST and TEM results, nor the several experiments that indicate phosphate dehydration plays an important role in modulating ^{31}P NMR relaxation.

Conclusion

In total, our experiments present strong evidence for the presence of phosphate assemblies in aqueous solutions driven by the dehydration of phosphate species. ^{31}P NMR relaxation and CEST results both indirectly reveal the presence of phosphate assemblies in exchange with free ionic phosphates, whose population grows with increasing temperature. Cryo-TEM confirms the presence of these assemblies in both monophosphate and ADP solutions, with structures consistent with condensed spherical droplets. ^{31}P DOSY measurements, as well as the impact of PEG and cationic salts, all indicated that dehydration of phosphate species drives the formation of these assemblies. Our results suggest that this dehydration-driven clustering of phosphates may be present in numerous species with exposed phosphate groups at a wide range of solution conditions, including those with biological relevance. Given these findings, and the ubiquity of phosphates in biological

systems, we propose that such clusters should be considered in the interpretation of both *in vivo* and *in vitro* experiments involving phosphate group-containing biomolecules.

Materials and Methods

Potassium phosphate monobasic (MW 136.09) and sodium phosphate monobasic (MW 119.98) were acquired from Fisher Scientific. Sodium phosphate tribasic (MW 163.94) was acquired from Acros Organics. Potassium pyrophosphate (MW 330.34) was acquired from Sigma-Aldrich. Adenosine 5'-diphosphate orthopotassium salt dihyrdate (MW 501.32) was acquired from Alfa Aesar. Adenosine 5'-triphosphate disodium salt hydrate (MW 551.14 anhydrous) was obtained from Sigma. Polyethylene glycol (MW 6K) was acquired from Fluka. Potassium chloride (MW 74.55), sodium chloride (MW 58.44), and ammonium chloride (MW 53.49) were acquired from Fisher Chemical. All samples prepared at room temperature. When not explicitly mentioned, the pH values were adjusted to 4.4 with HCl and NaOH to coincide with the native dissolved pH values found for monobasic orthophosphate. Every sample was dissolved in 600 to 700 uL of 90% Milli-Q water and 10% D_2O for locking purposes.

Adenosine 5'-diphosphate sodium salt (MW 427.20), sodium phosphate dibasic (MW 141.96), and coenzyme A sodium salt hydrate (MW 767.53) used for CEST were acquired from Sigma-Aldrich. All samples prepared at room temperature. The pH values of the solutions were adjusted to 4.4 with HCl and NaOH in order to make them coincide with the native dissolved pH values found for orthophosphate. The real concentrations of the solutions were determined from the absolute integrations of the ^{31}P peaks in the 1D NMR spectra.

NMR Experiments. Solution NMR relaxation experiments were performed on a Bruker Avance NEO 500 MHz spectrometer with a CryoProbe Prodigy BBO probe, using Wilmad-LabGlass 5 mm Thin Wall Precision NMR tubes. T_1 relaxation was measured with a standard inversion-recovery pulse sequence and T_2 relaxation was measured using a CPMG sequence. Delays varied depending on sample conditions (temperature, pH, and concentrations of salts and polyethlyene glycol (PEG)).

T_1 and T_2 delays were experimentally modulated such that the final two points for T_1 curves fully recovered and the final point for T_2 curves were less than 5% of the initial intensity. T_1 relaxation times were determined by employing the TopSpin 4.0.6 T1/T2 dynamics module. T_2 relaxation times were determined by MestReNova monoexponential fitting. FWHM was determined by taking a 45°pulse and employing TopSpin 4.0.6 PEAKW command. For each spectrum, a single scan was acquired with 40000 data points to cover a spectral window of 10000 Hz (49.4 ppm). An AU program was created to ensure temperature equalisation uniformity which included a ten minute temperature equilibration time and autoshimming was applied continuously before and throughout acquisition.

Diffusion ordered spectroscopy (DOSY) measurements were taken on a 300 MHz SWB Bruker spectrometer with a single gradient along the z-axis. DOSY is an experimental that uses the Pulsed Field Gradient NMR (PFG-NMR) technique to extract diffusion coefficients for each NMR signal present in a sample. PFG-NMR measures particle diffusion by using a spin-echo pulse sequence in combination with a magnetic field gradient. As particles diffuse during the spin-echo sequence, they experience a slightly different field due to the gradient, and the spin-echo is unable to completely rephase the signal. This dephasing causes an attenuated signal intensity, which depend on the strength of the gradient, g, and the diffusion coefficient, D of the species as $\psi(g, D) = Exp(-Dg^2\gamma^2\delta^2(\Delta - \delta/3))$ where γ is the gyromagnetic ratio of the nucleus, δ is the width of the gradient pulse, and Δ is the time between gradient pulses (34). By measuring this signal attenuation at several gradient strengths, one is able to fit the attenuation function to recover the diffusion coefficient of the associated species at each NMR line.

Measurements were taken at 293 K, 343 K, and again at 293 K after the sample had cooled. Capillaries were used at elevated temperatures to suppress convection. At 293 K, 32 scans with a 90°pulse were acquired with 16384 data points to cover a spectral window of 6068 Hz (49.9 ppm) for gradient strength, and at 343 K, 64 scans with a 90°pulse were acquired for each gradient strength with the same spectral conditions as above. At each temperature, data was taken using 16 linearly spaced gradient strengths such that the final spectrum had an intensity less than 5% of the first's. These decays were then fit in the TopSpin 4.0.6 T1/T2 relaxation module to extract a diffusion coefficient. The Stokes-Einstein relation was then used to convert this to a hydrodynamic diameter.

NMR chemical exchange saturation transfer (CEST) experiments were performed on a Bruker 500 MHz (11.7 T) NMR spectrometer equipped with a broadband observe (BBO) probe. The 90° pulse duration ranged from 10 to 12 us depending on ionic strength of the solution. Saturation was performed by continuous wave (cw) irradiation of 5 s duration with field strengths of 1.16 μT to 8.69 μT (corresponding to nutation frequencies of 20 Hz to 150 Hz). The recycling delay was set to 5 s. Following cw irradiation, a 90° pulse is used for spectral readout. The temperature dependence of CEST measurements were taken with the irradiation power of 150 Hz at 298 K, 313 K, 333 K, and 353 K, and the irradiation power dependence of CEST measurements were taken at 298 K with nutation frequencies of 20 Hz, 30 Hz, 50 Hz, and 150 Hz. At each measurement, 8 scans with a 90°pulse were acquired. The scanned frequency ranged from -1000 Hz to 1400 Hz with a step size of 50 Hz.

Control experiments were performed to rule out the influence of temperature gradients or convection on the results. Relaxation rates were found to be the same in samples containing capillaries (used to curb convection, if it exists), and chemical shift imaging was used to verify that the linewidths were the same in different z-positions in the sample.

cryo-TEM experiments. Phosphate solutions were vitrified using an FEI Vitrobot Mark IV for vitrification in liquid ethane. The cryo-TEM was performed using Gatan 626 Cryo transfer holder with liquid nitrogen by ThermoFisher Talos G2 200X TEM/STEM at 200 kV with a Ceta II CMOS camera for bright field imaging.

ACKNOWLEDGMENTS. AJ acknowledges support from the U.S. National Science Foundation, award no. CHE 2108205. This work was supported in part through the NYU IT High Performance Computing resources, services, and staff expertise. JSS, MN, and SH acknowledge the support of Dr. Hongjun Zhao, director of the NMR facility for the UCSB Department of Chemistry and Biochemistry and the support of NSF Major Research Instrumentation award, MRI-1920299, for magnetic resonance instrumentation. The contributions of JS and the NMR relaxometry, DOSY, and cryo-TEM are funded by the Heising-Simons Foundation. This material is based upon work supported by the National Science Foundation Graduate Research Fellowship under Grant No. 1650114. The authors acknowledge the use of the research facilities within the California NanoSystems Institute, supported by the University of California, Santa Barbara and the University of California, Office of the President. The MRL Shared Experimental Facilities are supported by the MRSEC Program of the NSF under Award No. DMR 1720256; a member of the NSF-funded Materials Research Facilities Network.

1. A Bangham, Membrane models with phospholipids. *Prog. Biophys. Mol. Biol.* **18**, 29–95 (1968).
2. MS Bretscher, Membrane structure: Some general principles. *Science* **181**, 622–629 (1973).
3. N Blumenthal, A Posner, Hydroxyapatite: Mechanism of formation and properties. *Cal. Tis Res.* **13**, 235–243 (1973).
4. H Schröder, L Kurz, W Müller, B Lorenz, Polyphosphate in bone. *Biochem. (Moscow)* **65**, 296–303 (2000).
5. L Wang, GH Nancollas, Calcium orthophosphates: Crystallization and dissolution. *Chem. Rev.* **108**, 4628–4669 (2008) PMID: 18816145.
6. JR Knowles, Enzyme-catalyzed phosphoryl transfer reactions. *Annu. Rev. Biochem.* **49**, 877–919 (1980) PMID: 6250450.
7. PP Dzeja, A Terzic, Phosphotransfer networks and cellular energetics. *J. Exp. Biol.* **206**, 2039–2047 (2003).
8. RA Meyer, HL Sweeney, MJ Kushmerick, A simple analysis of the "phosphocreatine shuttle". *Am. J. Physiol. Physiol.* **246**, C365–C377 (1984) PMID: 6372517.
9. GC Bogdanis, ME Nevill, LH Boobis, HK Lakomy, Contribution of phosphocreatine and aerobic metabolism to energy supply during repeated sprint exercise. *J. Appl. Physiol.* **80**, 876–884 (1996) PMID: 8964751.

10. A McLaughlin, et al., Application of 31p nmr to model and biological membrane systems. *FEBS Lett.* **57**, 213–218 (1975).
11. E Burnell, P Cullis, B de Kruijff, Effects of tumbling and lateral diffusion on phosphatidylcholine model membrane 31p-nmr lineshapes. *Biochimica et Biophys. Acta (BBA) - Biomembr.* **603**, 63–69 (1980).
12. Y Su, WF DeGrado, M Hong, Orientation, dynamics, and lipid interaction of an antimicrobial arylamide investigated by 19f and 31p solid-state nmr spectroscopy. *J. Am. Chem. Soc.* **132**, 9197–9205 (2010).
13. C Ho, JA Magnuson, JB Wilson, NS Magnuson, RJ Kurland, Phosphorus nuclear magnetic resonance studies of phosphoproteins and phosphorylated molecules. ii. chemical nature of phosphorus atoms in Î±8-casein b and phosvitin. *Biochemistry* **8**, 2074–2082 (1969) PMID: 5814938.
14. MHJ Seifert, et al., Phosphorylation and flexibility of cyclic-amp-dependent protein kinase (pka) using 31p nmr spectroscopy. *Biochemistry* **41**, 5968–5977 (2002) PMID: 11993991.
15. J Ren, B Yang, S A.D., M C.R., Exchange kinetics by inversion transfer: integrated analysis of the phosphorus metabolite kinetic exchanges in resting human skeletal muscle at 7 t. *Magn. resonance medicine* **73**, 1359–1369 (year?).
16. M Hupfer, R Gtichter, RR Ruegger, Polyphosphate in lake sediments: 31p nmr spectroscopy as a tool for its identification. *Limnol. Oceanogr.* **40**, 610–617 (1995).
17. LB Staal, et al., Extraction and quantification of polyphosphates in activated sludge from waste water treatment plants by 31p nmr spectroscopy. *Water Res.* **157**, 346–355 (2019).
18. EMM Weber, et al., Assessing the onset of calcium phosphate nucleation by hyperpolarized real-time nmr. *Anal. Chem.* **92**, 7666–7673 (2020) PMID: 32378878.
19. MA Swartz, PJ Tubergen, CD Tatko, RA Baker, Experimental determination of pka values and metal binding for biomolecular compounds using 31p nmr spectroscopy. *J. Chem. Educ.* **95**, 182–185 (2018).
20. Z SzabÃ³, Multinuclear nmr studies of the interaction of metal ions with adenine-nucleotides. *Coord. Chem. Rev.* **252**, 2362–2380 (2008) Applications of NMR to Inorganic and Organometallic Chemistry.
21. RK Brow, CC Phifer, GL Turner, RJ Kirkpatrick, Cation effects on 31p mas nmr chemical shifts of metaphosphate glasses. *J. Am. Ceram. Soc.* **74**, 1287–1290 (1991).
22. J Iwahara, YS Jung, GM Clore, Heteronuclear nmr spectroscopy for lysine nh3 groups in proteins:â unique effect of water exchange on 15n transverse relaxation. *J. Am. Chem. Soc.* **129**, 2971–2980 (2007) PMID: 17300195.
23. Z Luz, S Meiboom, Rate and mechanism of proton exchange in aqueous solutions of phosphate buffer. *J. Am. Chem. Soc.* **86**, 4764–4766 (1964).
24. HY Carr, EM Purcell, Effects of diffusion on free precession in nuclear magnetic resonance experiments. *Phys. Rev.* **94**, 630–638 (1954).
25. S Meiboom, D Gill, Modified Spin-Echo Method for Measuring Nuclear Relaxation Times. *Rev. Sci. Instruments* **29**, 688–691 (1958).
26. N Bloembergen, EM Purcell, RV Pound, Relaxation effects in nuclear magnetic resonance absorption. *Phys. Rev.* **73**, 679–712 (1948).
27. J Fraústo da Silva, R Williams, *The Biological Chemistry of the Elements: The Inorganic Chemistry of Life*. (Oxford University Press, Oxford), (1997).
28. JP Yesinowski, RJ Sunberg, JJ Benedict, ph control and rapid mixing in spinning nmr samples. *J. Magn. Reson. (1969)* **47**, 85–90 (1982).
29. TR Krawietz, et al., Solid phosphoric acid catalyst:â a multinuclear nmr and theoretical study. *J. Am. Chem. Soc.* **120**, 8502–8511 (1998).
30. NJ Anthis, GM Clore, Visualizing transient dark states by nmr spectroscopy. *Q. Rev. Biophys.* **48**, 35–116 (2015).
31. JM Edwards, et al., 19f dark-state exchange saturation transfer nmr reveals reversible formation of protein-specific large clusters in high-concentration protein mixtures. *Anal. Chem.* **91**, 4702–4708 (2019) PMID: 30801173.
32. P Vallurupalli, G Bouvignies, LE Kay, Studying âinvisibleâ excited protein states in slow exchange with a major state conformation. *J. Am. Chem. Soc.* **134**, 8148–8161 (2012) PMID: 22554188.
33. IAL Lim, et al., Quantitative magnetic susceptibility mapping without phase unwrapping using wassr. *NeuroImage* **86**, 265–279 (2014).
34. C Johnson, Diffusion ordered nuclear magnetic resonance spectroscopy: principles and applications. *Prog. Nucl. Magn. Reson. Spectrosc.* **34**, 203–256 (1999).
35. A Eiberweiser, A Nazet, G Hefter, R Buchner, Ion hydration and association in aqueous potassium phosphate solutions. *The J. Phys. Chem. B* **119**, 5270–5281 (2015) PMID: 25826464.
36. M Gerstein, C Chothia, Packing at the protein-water interface. *Proc. Natl. Acad. Sci.* **93**, 10167–10172 (1996).
37. M D'Agostino, et al., On the reliability of negative heat capacity measurements. *Nucl. Phys. A* **699**, 795–818 (2002).
38. D Marenduzzo, K Finan, PR Cook, The depletion attraction: an underappreciated force driving cellular organization. *J. Cell. Biol.* **175**, 681–686 (2016) PMID: 17145959.
39. A Bondi, van der waals volumes and radii. *The J. Phys. Chem.* **68**, 441–451 (1964).
40. S Park, et al., Dehydration entropy drives liquid-liquid phase separation by molecular crowding. *Commun. Chem.* **3**, 83 (2020).
41. S Großhans, G Wang, J Hubbuch, Water on hydrophobic surfaces: mechanistic modeling of polyethylene glycol-indcued protein precipitation. *Bioprocess Biosyst. Eng.* **42**, 513–520 (2019).
42. Y Zhang, PS Cremer, Interactions between macromolecules and ions: the hofmeister series. *Curr. Opin. Chem. Biol.* **10**, 658–663 (2006) Model systems / Biopolymers.
43. HI Okur, et al., Beyond the hofmeister series: Ion-specific effects on proteins and their biological functions. *The J. Phys. Chem. B* **121**, 1997–2014 (2017) PMID: 28094985.